Superstructures of lipids and graphene

Macedo Coelho Lima, L.

CHAPTER 2

Graphene-stabilized lipid monolayer heterostructures: a novel biomembrane superstructure

Chemically defined and electronically benign interfaces are attractive substrates for graphene and other two-dimensional materials. Here, lipid monolayers are introduced as an alternative, structurally ordered, and chemically versatile support for graphene. Deposition of graphene on the lipids resulted in a more ordered monolayer than regions without graphene. The lipids also offered graphene a more uniform and smoother support, reducing graphene hysteresis loop and the average value of the charge neutrality point under applied voltages. Our approach promises to be effective towards measuring experimentally biochemical phenomena within lipid monolayers and bilayers.

This chapter was published as a full article: Lia M. C. Lima, Wangyang Fu, Lin Jiang, Alexander Kros and Grégory F. Schneider, *Nanoscale*, **2016**, 8, 18646-8653

2.1 Introduction

Graphene[1] is typically supported – sometimes sandwiched – with other two-dimensional (2D) materials to promote higher mobility,[2] to ensure the reproducibility in electrical performances,[3] and to prevent environmental contamination.[4] Frequently composed of inorganic, hard and crystalline materials, the so called van der Waals heterostructures have emerged as a route to design new and remarkably complex layer-by-layer films of 2D materials, including graphene.[5] For example, the atomically flat hexagonal boron nitride (hBN) is frequently used as a support for graphene yielding a very high graphene electron mobility, in comparison with a Si/SiO_2 substrate which has a high surface roughness.[6] Alternatively, removing the hard substrates underneath graphene, i.e., suspending graphene, also improves the electron mobility of graphene, although the architecture and the methods of characterization are still limited.[7]

Nevertheless, one challenge associated with 2D materials as supporting and sandwiching layers is their limited chemical diversity, functions, and inherent inorganic nature. The possibility of combining graphene with soft, dynamic and molecular self-assembled monolayers is therefore of high interest as an organic alternative to inorganic 2D materials and could provide a versatile platform for applications, such as biosensors, drug delivery systems or cellular devices.[8]

Lipids – the main constituents of cell membranes – are amphiphilic molecules that can self-assemble and form stable quasi two dimensional fluidic membrane structures.[9] Lipids can spread on graphene,[10] however little is known on the formation, stability and molecular structure of lipid molecules surrounding graphene.[10-17] Mainly, studies focused on graphene oxide (GO), as both lipid vesicles and GO form stable suspensions in aqueous environments.[18] GO is an easily accessible form of graphene, suitable to study the influence of oxidation states on the chemical characteristics of GO-lipid assemblies, at the cost of lower electron mobility, higher chemical reactivity, oxygen doping, and surface/edge inhomogeneities. Being negatively charged, GO has a particular affinity with positively charged lipid head groups,[19] highlighting the importance of electrostatic interactions in the assembly process.[20] Pristine graphene, however, does not contain charges on the basal plane therefore minimizing electrostatic interactions and favoring hydrophobic interactions between lipid tails and graphene at the

interface.[21] To understand and quantify the interactions between lipid tails and graphene, an approach is that graphene crowd surfs directly on the lipid chains, and measure at the same time the electrical properties of graphene and the molecular structure of the lipids, for example, using infrared spectroscopy.

In this chapter we investigate the stability and structure of the lipid monolayer placed underneath graphene and report that graphene affects the conformation of a lipid monolayer, yielding a rearrangement of the lipids into a more ordered and more compact supramolecular conformation. Remarkably, attenuated transmission reflectance infrared spectroscopy (ATR-IR) and ellipsometry demonstrate an increase of the absorbance intensity and of the thickness of the lipid monolayer in presence of graphene, respectively. Our finding suggests a high affinity between the lipid tails and the graphene basal plane promoting a favorable heterostructure for biosensing applications, and represents the first step towards embedding graphene experimentally into the hydrophobic core of a lipid bilayer as proposed by recent molecular dynamics simulations reporting the favorable stabilization of such sandwiched structure.[22-23]

2.2 Results and discussion

One straightforward approach to form and study a graphene-lipid monolayer interface is to pre-form a well-packed monolayer of lipids on a known substrate, such as Si/SiO_2 and transfer a graphene layer on top. A well-established route to build an ordered lipid monolayer is by applying the Langmuir-Blodgett technique[24] using 1,2-dipalmitoyl-*sn*-glycero-3-phosphocholine (DPPC) and 1% of 1,2-dipalmitoyl-*sn*-glycero-3-phosphoethanolamine-N-(lissamine rhodamine B sulfonyl) (Liss Rhod PE) (Figure 2.1). First, the mixture of lipids is dissolved in an organic solution of chloroform/methanol (3:1) and is subsequently deposited dropwise at the air-water interface of the Langmuir trough. By further compressing this unordered lipid phase (i.e. in a gas phase (G), Figure 2.1a) to specific surface pressures, a very compact lipid monolayer can be formed and transferred to any arbitrary substrate.[25] In this study, the lipids were compressed to a surface pressure (π) of 30 mN/m – to form a compact and stable monolayer – and thereafter transferred to a Si/SiO_2 substrate by retracting the substrate out of the trough at maximum compression. A chemical vapor deposition (CVD) graphene layer was then transferred above the lipid film by bringing into contact the lipid

film with graphene floating on ammonium persulfate solution (APS, 0.5 M). The sample was immediately rinsed with ultrapure water to remove traces of APS (see Appendix I).

Figure 2.1a shows the surface pressure (π) – area isotherm of DPPC:Liss Rhod PE (99:1) (solid line) on a pure water sub-phase and the subsequent decompression of the Langmuir film (dashed line) after the transfer of the lipid monolayer onto the Si/SiO_2 substrate.

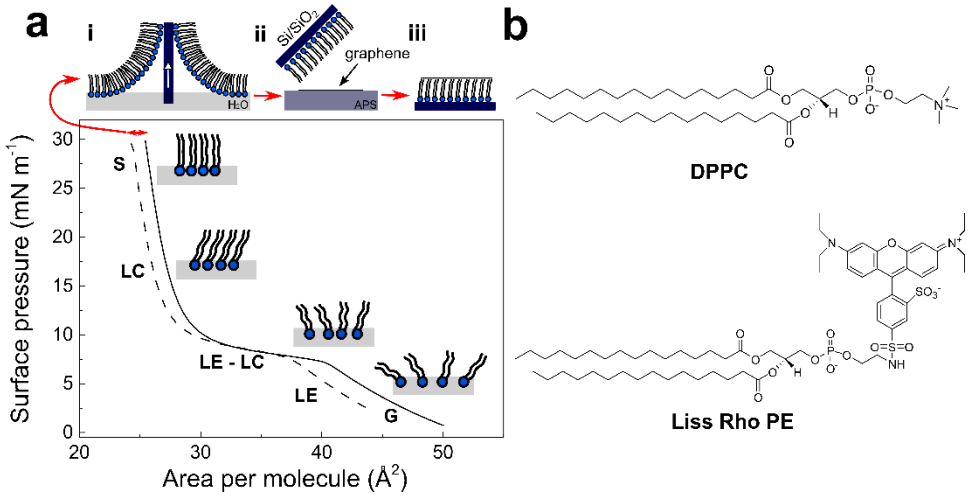

Figure 2.1. Lipid monolayer assembly and transfer of graphene. a) Surface pressure – area (π-A) compression isotherm of DPPC:Liss Rhod PE (99:1) monolayer (solid line) and the subsequent decompression (dashed line) after the transfer of the lipid monolayer on a Si/SiO_2 substrate (see top inset, step i). The different lipidic phases are: G, gaseous state; LE, liquid expanded state; LC, liquid condensed state; and S, solid state. In a last step graphene is transferred on top of the lipid monolayer from an ammonium persulfate solution (APS) (see top inset, step ii-iii). b) Molecular structure of the two lipids used in this work: 1,2-dipalmitoyl-*sn*-glycero-3-phosphocholine (DPPC) and 1,2-dipalmitoyl-*sn*-glycero-3-phosphoethanolamine-N-(lissamine rhodamine B sulfonyl) (Liss Rhod PE).

The lipid monolayer was compressed until a π of 30 mN/m passing through distinct separate phases characteristic of phospholipid molecules. In the first step, the lipids spread at the air-water interface yielding a gaseous state (G) due to the small intermolecular forces between the individual lipid molecules resulting from the large distance between molecules. As the mobile barriers of the Langmuir

trough start to compress, the available area per molecule and the intermolecular distance between the lipids decreases, resulting in the transition from the gaseous to a liquid expanded state (LE). After further compression, the molecules undergo a phase transition from a fluidic to a condensed phase. This liquid expanded (LE) – liquid condensed (LC) phase transition is characterized by a different aggregation state where the lipids present a strong lateral cohesion and a well-defined orientation. Finally, when the available area of the monolayer is further reduced, the lipid molecules self-organize in a perfectly ordered and stable monolayer, called the solid state (S).[26] At this stage, the well-packed lipid monolayer is transferred to the Si/SiO_2 substrate, resulting in a shift in the compression isotherms from which the transfer ratio of the lipids on the substrate is determined (Figure 2.1a, dashed line, red arrow; see Appendix I).

Optical and fluorescence microscopy measurements of the lipid monolayer and the subsequent lipid-graphene assembly are shown in Figure 2.2. A homogenous and continuous fluorescence layer is observed on Si/SiO_2 substrate (Figure 2.2a). Next, graphene was transferred onto the lipid monolayer resulting in a strong fluorescence quenching of the rhodamine B dye.[27] Note that millimeter sized graphene domains are observed, even without the need of a polymer such as PMMA for the transfer, as shown by Figure 2.2b and 2.2c.[28] The cracks on the basal plane of graphene are advantageous to image graphene using fluorescence quenching microscopy.[29] Remarkably, after rinsing with ultrapure water (to remove APS traces), the lipids underneath the graphene area remained intact, as confirmed by infrared spectroscopy and ellipsometry (Figure 2.3a), suggesting that graphene acts as a shield that prevent the lipids from getting rinsed off and protecting them from the environment (Figure 2.2b).

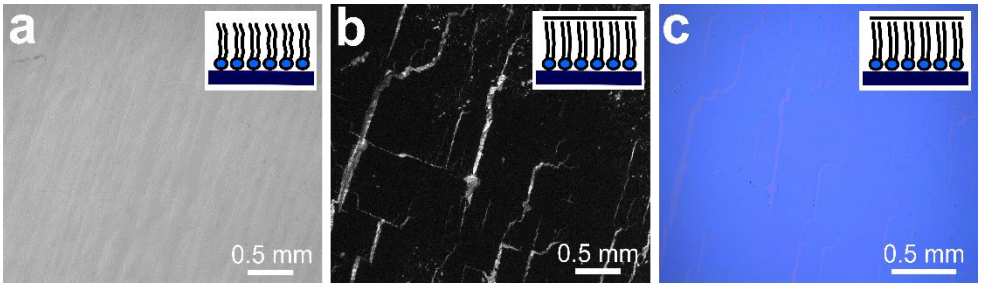

Figure 2.2. Microscopy imaging of the lipids and of the lipid-graphene heterostructure. a) Fluorescence image of DPPC:Liss Rhod PE (99:1) monolayer on Si/SiO_2 substrate. b) Fluorescence image after transferring graphene on top of the lipid monolayer. c) The corresponding optical image on the same graphene area of 2.2b.

In order to characterize the molecular structure and organization of the lipids, we performed attenuated total reflectance infrared (ATR-IR) spectroscopy measurements. Figure 2.3a shows the absorption bands characteristic for the stretching vibrations of the lipid acyl chains for the lipid monolayer (black line) and for the lipid-graphene assembly (red line).[30] The presence of these peaks confirms that the lipids remained underneath the graphene even after the extensive rising steps. Depending on whether the lipids are in contact or not with graphene, a shift in the wavenumber of the peak maximum is observed, characteristic for changes in the lipid conformation (i.e., a shift to lower wavenumber is often observed when the lipids within the monolayer are becoming more ordered).[31] Additionally, a shift was observed in the asymmetric methylene vibration (CH_2) from ~2915 to 2912 cm^{-1} and in the symmetric methylene vibration (CH_2) from ~2848 to 2844 cm^{-1}, respectively. Furthermore the intensity of the asymmetric and symmetric CH_2 bands of the lipid-graphene assembly increased. The observed shift is attributed to a change of the physical properties of the lipids film, where the frequencies of CH_2 stretching vibrations are known to decrease if lipids are well packed. An elongation of the lipid acyl chains will also yield an increase of intensity of the band. As the CH_2 frequency decreases, the lipid hydrocarbon chain order increases, suggesting a change from *gauche* to *trans* conformation of the lipid chains.[32] The molecules are closer to each other, have less freedom to vibrate and therefore lead to a decrease of the wavenumber. Thus, the lipids underneath graphene present a crystalline structure with presumably very restricted diffusional mobility.[31-33] At

this stage of the experiment, we therefore considered that graphene enters into – what we call – a 'crowd surfing' mode, either static or dynamic.

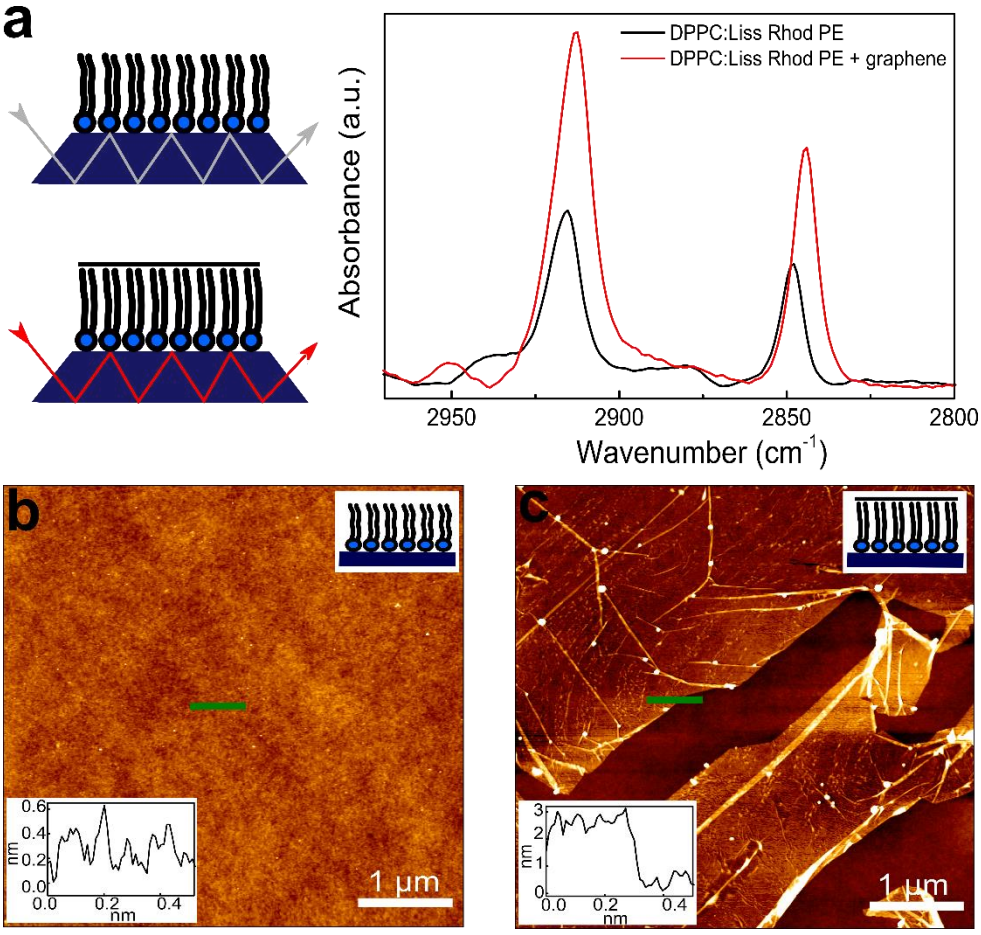

Figure 2.3. Attenuated total reflectance infrared (ATR-IR) and atomic force microscopy (AFM) characterization of the lipid-graphene heterostructure on a Si/SiO_2 substrate. a) ATR-IR absorption bands of CH_2 stretching vibrations of the lipid acyl chains before (black) and after (red) transferring graphene on top of a lipid monolayer transferred by Langmuir-Blodgett onto a Si/SiO_2 substrate. b) AFM intermittent contact mode image in air at room temperature of a DPPC:Liss Rhod PE (99:1) monolayer on Si/SiO_2 substrate and c) after transferring graphene on top of the lipid monolayer. The insets are the corresponding height profiles (green lines).

To obtain further information on the change of conformation of the lipid molecules upon their interaction with graphene, we determined the thickness of the different layers composing the thin film by ellipsometry (see Appendix I). The thickness of the SiO_2 layer was determined to be 282.9 ± 1.4 nm.[34] Then, after depositing the lipid monolayer, the total thickness increased by 2.5 ± 0.4 nm, as expected for a lipid monolayer.[35] After transferring graphene on top of the lipid monolayer, the thickness of the lipid monolayer increased to 3.9 ± 0.9 nm. This expansion of the lipid acyl chains, as confirmed previously by ATR-IR, corresponds to the formation of a more ordered structure. The interactions of the hydrophobic lipid tails with the hydrophobic graphene transferred on top are most probably remarkably favorable.[10, 22] This increase of 1.4 nm, could also be expected if a bilayer would form, but this hypothesis is excluded as no more lipids were in contact with the sample during the sample preparation. Although an absolute increase in thickness of 1.4 nm is surprising giving the expected head-to-tail length of DPPC, it is evident that the lipids re-arrange in a more organized layer after interacting with graphene, as confirmed previously by ATR-IR. The graphene thickness measured was 0.4 ± 0.2 nm, in agreement with the transfer of a single monolayer graphene.

The atomic force microscopy (AFM) images and the corresponding height profiles of the lipid monolayer in air at room temperature before and after transferring graphene showed the presence of an homogenous monolayer of lipids (Figure 2.3b), and for this reason, no significant step height differences could be measured on the lipid monolayer. These results confirm the formation of a stable and compacted lipid layer on Si/SiO_2 substrate (Figure 2.1a). The transferred graphene sheet on top of the lipid monolayer showed very flat and continuous domains (Figure 2.3c) with only a few wrinkles and cracks, as shown by fluorescence microscopy (Figure 2.2b).[36]

Figure 2.4a shows the averaged Raman spectra for graphene on a Si/SiO_2 substrate (black line) and for graphene transferred above the lipid monolayer in air at room temperature (red line). The sharp, symmetric and intensive 2D peak (~2680 cm^{-1}) and G peak (~1580 cm^{-1}) indicates the presence of single layer graphene.[37] The weak D peak at 1350 cm^{-1} is commonly present in CVD graphene, revealing a reasonable graphene quality. Specifically, the G band has been generally considered as an important indicator of doping effect in graphene.[38-39] In

Figure 2.4b, the G peak of graphene (1585.8 cm^{-1}) blue shifts if lipids are present underneath (1589.0 cm^{-1}). Such blue shift can be attributed to the known p-doping of lipids,[37] or due to the presence of an adsorbed water layer[40] at the interface between graphene and the substrate.

The imaging of the G peak position, its full width at half maximum (FWHM) and the intensity ratio of I(2D)/I(G) are summarized in the mapping data shown in Figure 2.4c. The G peak shows a larger blue shift and a much narrower width in the presence of the lipids as seen by the overall more reddish plots. Furthermore, the ratio of I(2D)/I(G) decreases for the lipid-graphene assembly compare to graphene on Si/SiO_2 substrate. All of these evidences confirm the p-doping effect from the lipids underneath graphene.[41-42] It is also worth to notice that the lipid-graphene assembly presents a more evenly color distribution than those of graphene on Si/SiO_2, which demonstrates that the lipid monolayer underneath supplies a more uniform and smooth support to graphene.

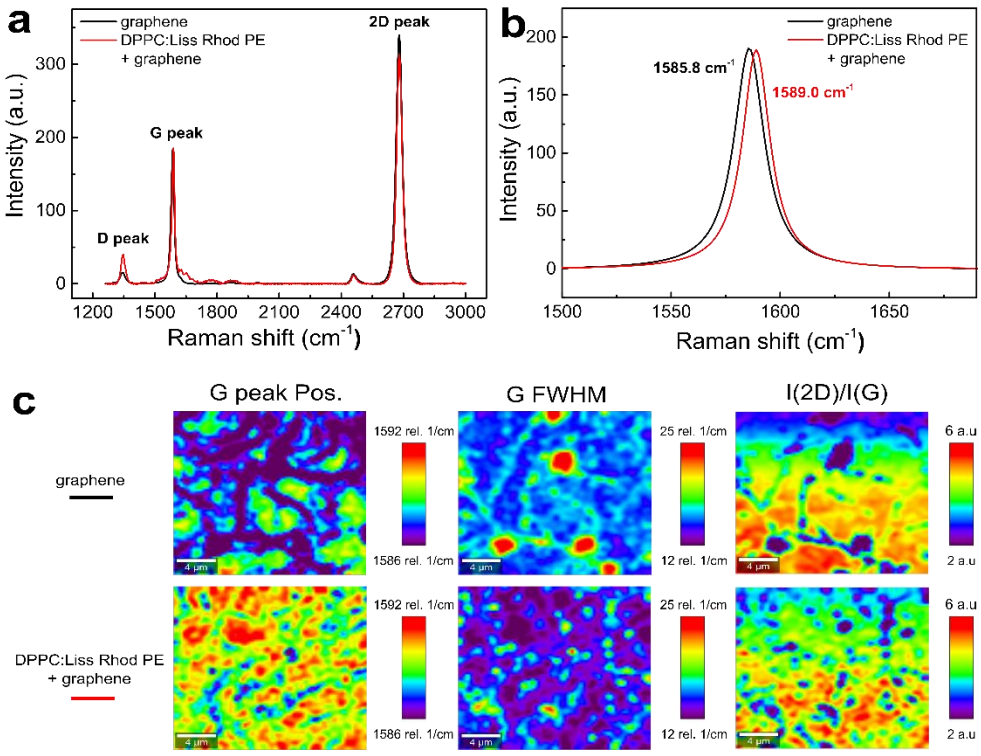

Figure 2.4. Raman spectroscopy and imaging of graphene and of lipid-graphene assembly. a) Raman spectra of graphene (black line) and of the lipid-graphene heterostructure (red line) on a Si/SiO_2 substrate. b) The Lorentz fitted G peak of the Raman spectra. c) Raman imaging of the G peak position, of its FWHM and the intensity ratio of I(2D)/I(G) for graphene (top) and for lipid-graphene heterostructure (bottom).

For electrical characterization of the lipid-graphene assembly, metal electrodes (chromium, 30 nm) were deposited on the CVD graphene above the lipid monolayer using a physical mask. As a control, we fabricated another graphene device directly on the Si/SiO_2 substrate using a PMMA assisted transfer method.[28]

The graphene device on bare Si/SiO_2 substrate exhibits a hysteresis of 10 V with an average charge neutrality point (CNP), V_{CNP} of about +30 V (Figure 2.5a, black line). The relatively large hysteresis and V_{CNP} can be ascribed to the well-known charge trap and p-doping effect of the Si/SiO_2 substrate.[43] Remarkably, the lipid monolayer favored the screening of the silicon substrate (Figure 2.5a, red line). As

a result, the electrical performances of the lipid-graphene device were improved with a reduced hysteresis loop (4 V) and a smaller average V_{CNP} (23 V). We note here that the decrease of the estimated carrier mobility of graphene on the lipid monolayer (430 cm^2/Vs compared to 640 cm^2/Vs on bare substrate) most likely originates from the incomplete surface coverage of graphene on the lipid monolayer. Another possible origin of this lower mobility is maybe the presence of more wrinkles as depicted in Figure 2.3c. The graphene coverage with the lipid-assisted transfer method was below 80%, whereas the graphene coverage on bare substrate was larger than 95% (observed by optical images). In addition, occasionally we also observed in our experiments that defective lipids (Langmuir-Blodgett transfer ratio < 1) degraded the performance of graphene device by introducing even more p-doping effect (with V_{CNP} > 80 V) and larger hysteresis (> 25 V) (Figure 2.5a, green line). We have repeated the electrical measurements for another lipid-graphene sample. This sample exhibited a carrier mobility of 570 cm^2/Vs, a hysteresis of 1.5 V, and a V_{CNP} of 8 V, closely resembling what we showed in Figure 2.5a. We noted here that we tested also a few defective samples. The carrier mobility, hysteresis, and V_{CNP} of these defective samples demonstrated a wide distribution of ~ 100-700 cm^2/Vs, ~ 6-11 V, and ~ 11-45 V, respectively.

In Figure 2.5b, the intensity ratio between the D peak and G peak I(D)/I(G) revealed the disorder and defects on graphene, which can be ascribed to effects of the substrate. These substrate effects are primarily due to the roughness of Si/SiO_2 substrate, the strain induced by the lipid monolayer underneath, and the possible adsorbed water layer at the Si/SiO_2-lipid interface. Compare to graphene on the lipid monolayer (Figure 2.5b, middle), the I(D)/I(G) ratio of graphene on defective lipids (Figure 2.5b, bottom) is more intense. A higher I(D)/I(G) ratio is in line with the larger field-effect hysteresis (25 V in case of defective lipids supporting graphene compared to 4 V in case of graphene on lipid monolayer) and the higher p-doping (i.e., larger average V_{CNP} of 80 V compared to 23 V for graphene on lipid monolayer). We note here that the I(D)/I(G) ratio of graphene on a bare Si/SiO_2 substrate (Figure 2.5b, top) was indeed less intensive than the one for graphene on a lipid monolayer (Figure 2.5b, middle). Nevertheless, we observed a less pronounced field-effect hysteresis (4 V in case of lipid monolayer supporting graphene compared to 10 V in case of graphene on the bare substrate) and a smaller average V_{CNP} (23 V compared to 30 V for graphene on the bare substrate),

which could be ascribed to the PMMA assisted transfer method we used for transferring graphene on bare substrate.

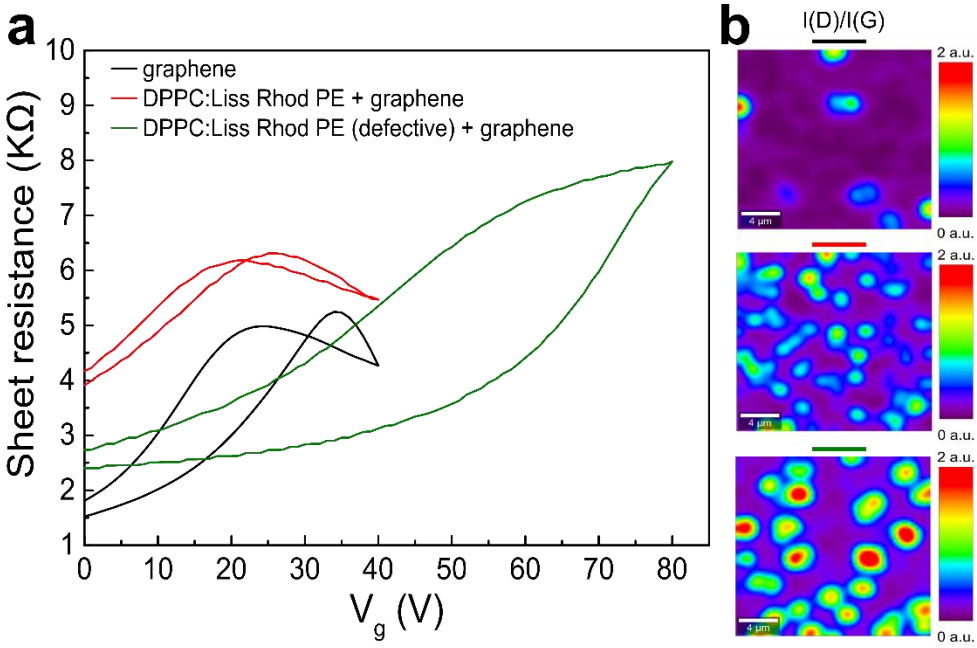

Figure 2.5. Effect of the lipid monolayer on the electrical measurements of graphene. a) The back gate voltage (Vg) dependent sheet resistance (R) of graphene on Si/SiO_2 substrate (black line), lipid-graphene assembly (red line), and on graphene with defective lipid monolayer (green line). b) Raman imaging of the intensity ratio of I(D)/I(G) for graphene on Si/SiO_2 substrate (top), lipid-graphene assembly (middle), and graphene with defective lipid monolayer (bottom).

2.3 Conclusions

The observation of a unique re-ordering of lipid molecules in the presence of graphene reveals an increase in the packing of the lipid monolayer as graphene crowd surfs on the lipid monolayer. Remarkably, lipids ameliorated the electrical performances of the graphene, which is of high interest for using lipids as alternative soft substrates for graphene. Additionally, the direct contact between graphene and lipids is particularly attracting for measuring biochemical phenomena, for example in-situ a lipidic layer. Future experiments investigating

different lipids with different charges, different phase transition temperatures, and different lipid packing will be essential to elucidate the potential sensitivity of graphene to even more subtle changes in (bio)molecular conformations. A practical benefit of the lipid monolayer is also that large millimeter sized and continuous graphene domains are supported, avoiding polymers or any contaminants usually used during typical graphene transfers.

Interfacing graphene with lipid molecules will offer a new sensing platform to chemically modulate the electrical properties of graphene by varying the lipids structure and is the first step towards sandwiching graphene within the hydrophobic core of a lipid bilayer (Chapter 3).

2.4 References

1. Novoselov, K. S.; Geim, A. K.; Morozov, S. V.; Jiang, D.; Zhang, Y.; Dubonos, S. V.; Grigorieva, I. V.; Firsov, A. A., Electric field effect in atomically thin carbon films. *Science* **2004,** *306* (5696), 666-669.

2. Dean, C. R.; Young, A. F.; Meric, I.; Lee, C.; Wang, L.; Sorgenfrei, S.; Watanabe, K.; Taniguchi, T.; Kim, P.; Shepard, K. L.; Hone, J., Boron nitride substrates for high-quality graphene electronics. *Nat. Nanotechnol.* **2010,** *5* (10), 722-726.

3. Xue, J.; Sanchez-Yamagishi, J.; Bulmash, D.; Jacquod, P.; Deshpande, A.; Watanabe, K.; Taniguchi, T.; Jarillo-Herrero, P.; Leroy, B. J., Scanning tunnelling microscopy and spectroscopy of ultra-flat graphene on hexagonal boron nitride. *Nat. Mater.* **2011,** *10* (4), 282-285.

4. Wang, L.; Meric, I.; Huang, P. Y.; Gao, Q.; Gao, Y.; Tran, H.; Taniguchi, T.; Watanabe, K.; Campos, L. M.; Muller, D. A.; Guo, J.; Kim, P.; Hone, J.; Shepard, K. L.; Dean, C. R., One-dimensional electrical contact to a two-dimensional material. *Science* **2013,** *342* (6158), 614-617.

5. Geim, A. K.; Grigorieva, I. V., Van der waals heterostructures. *Nature* **2013,** *499* (7459), 419-425.

6. Xue, J.; Sanchez-Yamagishi, J.; Bulmash, D.; Jacquod, P.; Deshpande, A.; Watanabe, K.; Taniguchi, T.; Jarillo-Herrero, P.; LeRoy, B. J., Scanning tunnelling microscopy and spectroscopy of ultra-flat graphene on hexagonal boron nitride. *Nat. Mater.* **2011,** *10*, 282.

7. Du, X.; Skachko, I.; Barker, A.; Andrei, E. Y., Approaching ballistic transport in suspended graphene. *Nat. Nanotechnol.* **2008,** *3*, 491.

8. Ferrari, A. C.; Bonaccorso, F.; Fal'ko, V.; Novoselov, K. S.; Roche, S.; Boggild, P.; Borini, S.; Koppens, F. H. L.; Palermo, V.; Pugno, N.; Garrido, J. A.; Sordan, R.; Bianco, A.; Ballerini, L.; Prato, M.; Lidorikis, E.; Kivioja, J.; Marinelli, C.; Ryhanen, T.; Morpurgo, A.; Coleman, J. N.; Nicolosi, V.; Colombo, L.; Fert, A.; Garcia-Hernandez, M.; Bachtold, A.; Schneider, G. F.; Guinea, F.; Dekker, C.; Barbone, M.; Sun, Z.; Galiotis, C.; Grigorenko, A. N.; Konstantatos, G.; Kis, A.; Katsnelson, M.; Vandersypen, L.; Loiseau, A.; Morandi, V.; Neumaier, D.; Treossi, E.; Pellegrini, V.; Polini, M.; Tredicucci,

A.; Williams, G. M.; Hee Hong, B.; Ahn, J.-H.; Min Kim, J.; Zirath, H.; van Wees, B. J.; van der Zant, H.; Occhipinti, L.; Di Matteo, A.; Kinloch, I. A.; Seyller, T.; Quesnel, E.; Feng, X.; Teo, K.; Rupesinghe, N.; Hakonen, P.; Neil, S. R. T.; Tannock, Q.; Lofwander, T.; Kinaret, J., Science and technology roadmap for graphene, related two-dimensional crystals, and hybrid systems. *Nanoscale* **2015,** *7*, 4598-4810.

9. van Meer, G.; Voelker, D. R.; Feigenson, G. W., Membrane lipids: Where they are and how they behave. *Nat. Rev. Mol. Cell. Biol.* **2008,** *9* (2), 112-124.

10. Hirtz, M.; Oikonomou, A.; Georgiou, T.; Fuchs, H.; Vijayaraghavan, A., Multiplexed biomimetic lipid membranes on graphene by dip-pen nanolithography. *Nat. Commun.* **2013,** *4*, 2591.

11. Wang, Y. Y.; Pham, T. D.; Zand, K.; Li, J.; Burke, P. J., Charging the quantum capacitance of graphene with a single biological ion channel. *ACS Nano* **2014,** *8* (5), 4228–4238.

12. Ang, P. K.; Jaiswal, M.; Lim, C. H. Y. X.; Wang, Y.; Sankaran, J.; Li, A.; Lim, C. T.; Wohland, T.; Barbaros, Ö.; Loh, K. P., A bioelectronic platform using a graphene−lipid bilayer interface. *ACS Nano* **2010,** *4* (12), 7387-7394.

13. Connelly, L. S.; Meckes, B.; Larkin, J.; Gillman, A. L.; Wanunu, M.; Lal, R., Graphene nanopore support system for simultaneous high-resolution afm imaging and conductance measurements. *ACS Appl. Mater. Interf.* **2014,** *6* (7), 5290-5296.

14. Yamazaki, K.; Kunii, S.; Ogino, T., Characterization of interfaces between graphene films and support substrates by observation of lipid membrane formation. *J. Phys. Chem. C* **2013,** *117* (37), 18913-18918.

15. Tabaei, S. R.; Ng, W. B.; Cho, S.-J.; Cho, N.-J., Controlling the formation of phospholipid monolayer, bilayer, and intact vesicle layer on graphene. *ACS Appl. Mater. Interfaces* **2016,** *8* (18), 11875-11880.

16. Tu, Y.; Lv, M.; Xiu, P.; Huynh, T.; Zhang, M.; Castelli, M.; Liu, Z.; Huang, Q.; Fan, C.; Fang, H.; Zhou, R., Destructive extraction of phospholipids from escherichia coli membranes by graphene nanosheets. *Nat. Nanotechnol.* **2013,** *8* (8), 594-601.

17. Luan, B.; Huynh, T.; Zhou, R., Complete wetting of graphene by biological lipids. *Nanoscale* **2016,** *8* (10), 5750-5754.

18. Hummers, W. S.; Offeman, R. E., Preparation of graphitic oxide. *J. Am. Chem. Soc.* **1958,** *80* (6), 1339-1339.

19. Li, S. H.; Stein, A. J.; Kruger, A.; Leblanc, R. M., Head groups of lipids govern the interaction and orientation between graphene oxide and lipids. *J. Phys. Chem. B* **2013,** *117* (31), 16150-16158.

20. Frost, R.; Jonsson, G. E.; Chakarov, D.; Svedhem, S.; Kasemo, B., Graphene oxide and lipid membranes: Interactions and nanocomposite structures. *Nano Lett.* **2012,** *12* (7), 3356-3362.

21. Rodriguez-Perez, L.; Herranz, M. A.; Martin, N., The chemistry of pristine graphene. *Chem. Commun.* **2013,** *49* (36), 3721-3735.

22. Titov, A. V.; Kral, P.; Pearson, R., Sandwiched graphene-membrane superstructures. *ACS Nano* **2010,** *4* (1), 229-234.

23. Mao, J.; Guo, R.; Yan, L.-T., Simulation and analysis of cellular internalization pathways and membrane perturbation for graphene nanosheets. *Biomaterials* **2014,** *35* (23), 6069-6077.

24. Yu, Z.-W.; Jin, J.; Cao, Y., Characterization of the liquid-expanded to liquid-condensed phase transition of monolayers by means of compressibility. *Langmuir* **2002,** *18* (11), 4530-4531.

25. Hirtz, M.; Fuchs, H.; Chi, L., Influence of substrate treatment on self-organized pattern formation by langmuir−blodgett transfer. *J. Phys. Chem. B* **2008,** *112* (3), 824-827.

26. Oncins, G.; Picas, L.; Hernández-Borrell, J.; Garcia-Manyes, S.; Sanz, F., Thermal response of langmuir-blodgett films of dipalmitoylphosphatidylcholine studied by atomic force microscopy and force spectroscopy. *Biophys. J.* **2007,** *93* (8), 2713-2725.

27. Arjmandi-Tash, H.; Jiang, L.; Schneider, G. F., Rupture index: A quantitative measure of sub-micrometer cracks in graphene. *Carbon* **2017,** *118*, 556-560.

28. Li, X.; Zhu, Y.; Cai, W.; Borysiak, M.; Han, B.; Chen, D.; Piner, R. D.; Colombo, L.; Ruoff, R. S., Transfer of large-area graphene films for high-performance transparent conductive electrodes. *Nano Lett.* **2009,** *9* (12), 4359-4363.

29. Kim, J.; Cote, L. J.; Kim, F.; Huang, J., Visualizing graphene based sheets by fluorescence quenching microscopy. *J. Am. Chem. Soc.* **2010,** *132* (1), 260-267.

30. Blume, A.; Kerth, A., Peptide and protein binding to lipid monolayers studied by ft-irra spectroscopy. *BBA-Biomembranes* **2013,** *1828* (10), 2294-2305.

31. Tatulian, S. A., Attenuated total reflection fourier transform infrared spectroscopy: A method of choice for studying membrane proteins and lipids. *Biochemistry (Mosc).* **2003,** *42* (41), 11898-11907.

32. Lewis, R. N. A. H.; McElhaney, R. N., Membrane lipid phase transitions and phase organization studied by fourier transform infrared spectroscopy. *BBA-Biomembranes* **2013,** *1828* (10), 2347-2358.

33. Small, D. M., Lateral chain packing in lipids and membranes. *J. Lipid Res.* **1984,** *25* (13), 1490-1500.

34. C. M. Herzinger, W. A. J., J. A. Woollam, Ellipsometric determination of optical constants for silicon and thermally grown silicon dioxide via a multi-sample, multi-wavelength, multi-angle investigation. *J. Appl. Phys.* **1998,** *86* (6), 3323-3336.

35. Yang, X. M.; Xiao, D.; Xiao, S. J.; Wei, Y., Domain structures of phospholipid monolayer langmuir-blodgett films determined by atomic force microscopy. *Appl. Phys. A* **1994,** *59* (2), 139-143.

36. Nemes-Incze, P.; Osváth, Z.; Kamarás, K.; Biró, L. P., Anomalies in thickness measurements of graphene and few layer graphite crystals by tapping mode atomic force microscopy. *Carbon* **2008,** *46* (11), 1435-1442.

37. Das, A.; Pisana S.; Chakraborty B.; Piscanec S.; Saha, S. K.; Waghmare, U. V.; Novoselov, K. S.; Krishnamurthy, H. R.; Geim, A. K.; Ferrari, A. C.; Sood, A. K., Monitoring dopants by raman scattering in an electrochemically top-gated graphene transistor. *Nat. Nanotechnol.* **2008,** *3* (4), 210-215.

38. Pisana, S.; Lazzeri, M.; Casiraghi, C.; Novoselov, K. S.; Geim, A. K.; Ferrari, A. C.; Mauri, F., Breakdown of the adiabatic born-oppenheimer approximation in graphene. *Nat. Mater.* **2007,** *6* (3), 198-201.

39. Yan, J.; Zhang, Y.; Kim, P.; Pinczuk, A., Electric field effect tuning of electron-phonon coupling in graphene. *Phys. Rev. Lett.* **2007,** *98* (16), 166802.

40. Tsukamoto, T.; Yamazaki, K.; Komurasaki, H.; Ogino, T., Effects of surface chemistry of substrates on raman spectra in graphene. *J. Phys. Chem. C* **2012,** *116* (7), 4732-4737.

41. Bruna, M.; Ott, A. K.; Ijäs, M.; Yoon, D.; Sassi, U.; Ferrari, A. C., Doping dependence of the raman spectrum of defected graphene. *ACS Nano* **2014,** *8* (7), 7432-7441.

42. Basko, D. M.; Piscanec, S.; Ferrari, A. C., Electron-electron interactions and doping dependence of the two-phonon raman intensity in graphene. *Phys. Rev. B* **2009,** *80* (16), 165413.

43. Lafkioti, M.; Krauss, B.; Lohmann, T.; Zschieschang, U.; Klauk, H.; Klitzing, K. v.; Smet, J. H., Graphene on a hydrophobic substrate: Doping reduction and hysteresis suppression under ambient conditions. *Nano Lett.* **2010,** *10* (4), 1149-1153.